Published by IOP Publishing for SISSA
Received: *October 8, 2008*
Revised: *December 15, 2008*
Accepted: *December 15, 2008*
Published: *January 15, 2009*

JHEP01(2009)038

$\mathcal{O}(\alpha\alpha_s)$ corrections to the $\gamma t\bar{t}$ vertex at the top quark threshold

Yuichiro Kiyo, Dirk Seidel and Matthias Steinhauser

Institut für Theoretische Teilchenphysik, Universität Karlsruhe (TH),
Karlsruhe Institute of Technology (KIT),
76128 Karlsruhe, Germany
E-mail: kiyo@particle.uni-karlsruhe.de, dirk.seidel@kit.edu, matthias.steinhauser@uka.de

Abstract: We compute the last missing piece of the two-loop $\mathcal{O}(\alpha\alpha_s)$ corrections to $\gamma t\bar{t}$ vertex at the $t\bar{t}$ threshold due to the exchange of a W boson and a gluon. This contribution constitutes a building block of the top quark threshold production cross section at electron positron colliders.

Keywords: Standard Model, Quark Masses and SM Parameters, Heavy Quark Physics.

Contents

1. Introduction

The top quark pair production close to the threshold is an important process at a future International Linear Collider (ILC). It can be used to determine top quark properties, like the mass m_t and the width Γ_t, but also the strong coupling α_s with high precision. This is in particular true for m_t where an uncertainty below 100 MeV can be obtained from a threshold scan of the cross section [1].

The feasibility of such high-precision measurements requires a theory prediction of the total cross section $\sigma(e^+e^- \to t\bar{t})$ with high accuracy (preferably $\delta\sigma/\sigma \leq 3\%$). The study of $t\bar{t}$ threshold production is performed in the framwork or non-relativistic QCD (NRQCD) [2] which separates the hard and soft scales involved in the process. In such a framework, one has two expansion parameters, α_s and the relative velocity v of the heavy quarks. The corrections are classified by the total power of α_s and v, i.e. N^{k}LO corections contain terms of order $\alpha_s^l v^m$ with $l+m=k$. The next-to-next-to-leading order calculation has been perormed in ref. [3]. Current estimates based on (partial) next-to-next-to-next-to-leading order (NNNLO) [4, 5] QCD corrections lead to an uncertainty of the order of 10%. Similar conclusions are obtained from the approach based on the resummation of logarithmically enhanced terms which has been considered in refs. [6, 7].

In order to reach a theory goal of $\delta\sigma/\sigma \leq 3\%$ it is necessary to include in the prediction next to the one-loop electroweak corrections, which are known since quite some time [8] (see also [9]), also higher order effects. The evaluation of $\mathcal{O}(\alpha\alpha_s)$ corrections has been

JHEP01(2009)038

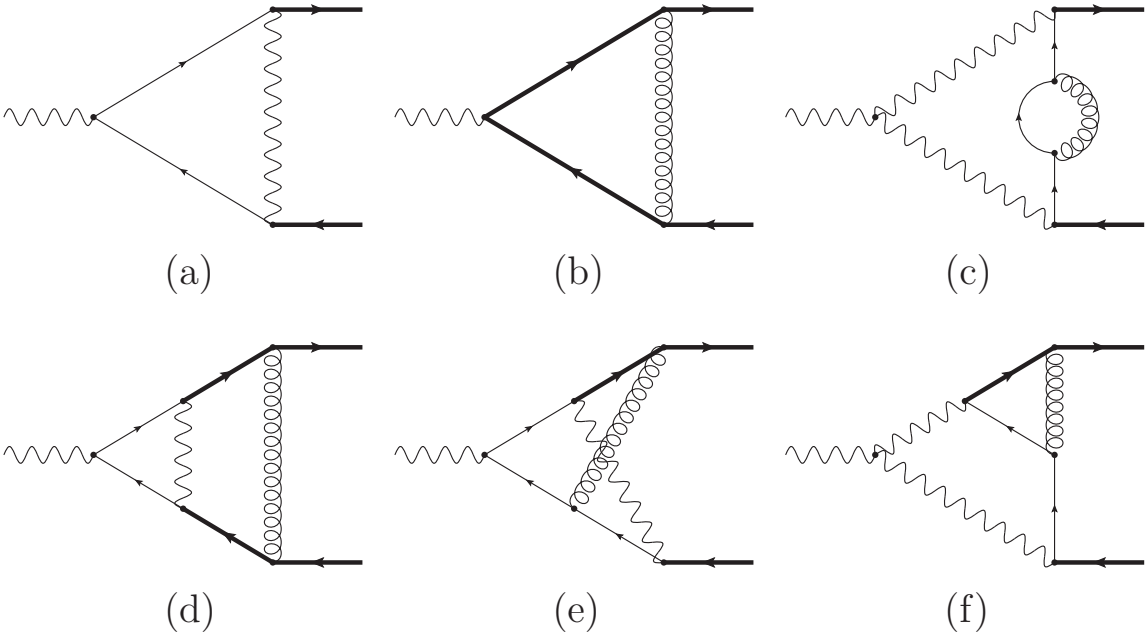

Figure 1: Sample Feynman diagrams contributing to the matching coefficient of the vector current at order α (a), α_s (b) and $\alpha\alpha_s$ (c)-(f). The thick (thin) straight lines represent top (bottom) quarks, wavy lines stand for W bosons and the curly ones for gluons.

started in ref. [10], where the two-loop mixed electroweak and QCD corrections to the matching coefficient of the vector current has been computed due to a Higgs or Z boson exchange in addition to a gluon. The current paper continues this enterprise and provides a result of $\mathcal{O}(\alpha\alpha_s)$ for the two-loop vertex diagrams mediated by a W boson and gluon exchange.[1] Sample diagrams can be found in figure 1. This completes the vertex corrections of order $\alpha\alpha_s$ — a building block for the top quark production cross section. Assuming the (numerically well justified) power counting $\alpha \sim \alpha_s^2$ one can see that these corrections are formally of NNNLO.

In order to complete the matching corrections of order $\alpha\alpha_s$ also the two-loop box diagrams contributing to $e^+e^- \to t\bar{t}$ have to be considered. Actually, only the proper combination of the box, vertex and self-energy contributions (the latter can, e.g., be found in refs. [11, 12]) forms a gauge independent set.

The remainder of the paper is organized as follows: In the next section we introduce our notation and derive the cross section formula for $e^+e^- \to t\bar{t}X$ near the $t\bar{t}$ threshold. We present a general formula which includes all radiative corrections of the Standard Model (SM). In section 3 we discuss some technical details of the two-loop computation and in section 4 we concentrate on the $\mathcal{O}(\alpha\alpha_s)$ corrections to the $\gamma t\bar{t}$ vertex and present our results. Section 5 contains our conclusions. Additional useful material concerning the one-loop expressions can be found in the appendix.

[1] Of course, in addition to the gauge boson also the corresponding Goldstone boson is taken into account.

JHEP01(2009)038

2. Threshold cross section

Within the framework of NRQCD the total cross section for the top quark production can be cast in the form

$$R\left(e_L^+ e_R^- \to t\bar{t}X\right) = \frac{8\pi}{s}\,\mathrm{Im}\big[\,(h_{R,V})^2\,H_V + (h_{R,A})^2\,H_A\big]\,, \tag{2.1}$$

where s is the square of the center-of-mass energy and $R(e_L^+ e_R^- \to t\bar{t}X)$ is the cross section normalized to $\sigma(e^+e^- \to \mu^+\mu^-) = (4\pi\alpha^2)/(3s)$. For illustration we consider in eq. (2.1) left-landed positrons and right-handed electrons. For $e_R^+ e_L^-$ in the initial state a similar expression is obtained by replacing R by L in eq. (2.1). Note that in the SM the initial states $e_R^+ e_R^-$ and $e_L^+ e_L^-$ are suppressed by a factor $(m_e/M_W)^2 \sim 10^{-10}$ and are thus negligible. We denote $h_{R,V}$ and $h_{R,A}$ by helicity amplitudes which absorb the matching coefficients representing the effective coupling of the effective operators. They take care of the hard part of the reaction. The first subscript of h refers to helicity of the electron, and the second one to the vector ($J_V^\mu = \bar{\psi}\gamma^\mu\psi$) or axial-vector coupling ($J_A^\mu = \bar{\psi}\gamma^\mu\gamma_5\psi$) of the gauge bosons to the top quark current.[2] The bound-state dynamics is contained in the so-called hadronic part which is denoted by H_V and H_A in eq. (2.1).

In the cross section formula (2.1) "Im" refers to those cuts which correspond to the $t\bar{t}X$ final state.[3] This means that we have to select special cuts which correspond to the final state we are interested in. This requires a dedicated study incorporating the experimental setup. For the one-loop electroweak correction this treatment was performed in [13]. In this paper we will not pursue this problem further (see also the discussion in the Conclusions).

The hadronic part is described by NRQCD [2]. For our purpose it is sufficient to re-write the vector current J_V^μ and the axial-vector current J_A^μ in terms of two-component NRQCD spinor fields ψ, χ, which correspond to non-relativistic top and anti-top quarks, respectively. This yields the following NRQCD currents

$$\begin{aligned} j_V^i &= \psi^\dagger\,\sigma^i\chi\,, \\ j_V^{(1/m^2),\,i} &= -\frac{1}{6m_t^2}\psi^\dagger\,\sigma^i(i\vec{D}\,)^2\,\chi\,, \\ j_A^i &= \frac{1}{2m_t}\,\psi^\dagger\,[\sigma^i, (\vec{\sigma}\,i\vec{D}\,)]\,\chi\,. \end{aligned} \tag{2.2}$$

With the help of the NRQCD equation of motion for top and anti-top quarks ($\psi^\dagger\sigma^i\,\vec{D}^{\,2}\chi = m_t\,i\partial_0(\psi^\dagger\sigma^i\chi)$) the $1/m^2$-suppressed vector current can be re-expressed in terms of j_V. Thus our matching relation between SM and NRQCD currents are given by

$$J_V = e^{2im_t x_0}\left(c_v - \frac{d_v}{6m_t}i\partial_0\right)\,j_V\,, \qquad J_A = e^{2im_t x_0}c_a\,j_A\,, \tag{2.3}$$

[2]The notation is basically adapted from ref. [8], however, we added a second subscript $F = V, A$ to incorporate the axial-vector coupling of the $Zt\bar{t}$ vertex (see eq. (2.5)).

[3]From the theoretical point of view one has a pure $t\bar{t}$ final state up to NNLO in QCD. Starting from NNNLO one has to include the real emission of a gluon. Once the electroweak sector is considered, final states like $(bW^+)\bar{t}$ need to be included, where (bW^+) has an invariant mass p_{bW}^2 in a range $|p_{\mathrm{bW}}^2 - m_t^2| \lesssim m_t\Gamma_t$.

with $c_v = d_v = c_a = 1$ at tree level. The hadronic part is defined by the current correlation function

$$H_F = i \sum_k \int \mathrm{d}x\, e^{iEx^0} \langle \Omega \,|\, \mathrm{T}\, j_F^{k\,\dagger}(x)\, j_F^k(0) \,|\Omega\rangle \qquad (F = V, A)\,, \tag{2.4}$$

where $E = \sqrt{s} - 2m_t$ and $|\Omega\rangle$ is the NRQCD vacuum state.

The evaluation of H_F requires to integrate out the low-energy modes of QCD, the soft, potential and ultrasoft gluons contained in NRQCD [14, 15]. For the top quark system this can be done perturbatively. In a first step one integrates out the soft and potential gluons which results in the effective field theory Potential NRQCD [16, 17]. The corresponding Lagrangian is known to NNNLO [18].[4] To integrate out nonrelativistic top and anti-top quark fields the Rayleigh-Schrödinger perturbation theory can be applied as was initiated in ref. [20] and performed to NNNLO for H_V and H_A in refs. [4] and [21], respectively. Integrating out the ultrasoft gluon was completed recently in ref. [5]. For the details of these steps we refer the reader to the original papers and references cited therein (see also refs. [22 – 26]).

In this paper we restrict ourselves to hard loop corrections to the production cross section, namely the corrections being parameterized as $h_{I,F}$. The tree-level expression[5] of the helicity amplitude $h_{I,F}$ is given by

$$\begin{aligned} h_{I,V}^{\mathrm{tree}} &= Q_e Q_t + \frac{s\,\beta_I^e\,\beta_V^t}{s - M_Z^2} \qquad \text{with} \qquad \beta_V^t = \frac{\beta_R^t + \beta_L^t}{2}\,, \\ \beta_I^f &= \frac{(T_3)_{f_I} - s_w^2 Q_f}{s_w c_w} \qquad (I = L/R)\,, \end{aligned} \tag{2.5}$$

where the β_I^f is the coupling of a fermion ($f = e, t$) to the Z boson, s_w is the sine of the weak-mixing ($c_w^2 = 1 - s_w^2$), and electric and iso-spin charges for top quark and electron are given by

$$Q_e = -1\,, \quad Q_t = 2/3\,, \quad (T_3)_{t_L} = 1/2\,, \quad (T_3)_{e_L} = -1/2\,, \quad (T_3)_{f_R} \equiv 0\,. \tag{2.6}$$

In the following the abbreviation $T_3^f \equiv (T_3)_{f_L}$ will be used. $h_{I,A}$ can be obtained by substituting β_V^t by $\beta_A^t = (\beta_R^t - \beta_L^t)/2$ in formula (2.5).

Let us now explain how hard loop corrections within the SM can be incorporated into the helicity amplitude $h_{I,F}$. To this end we organize the corrections as

$$\begin{aligned} h_{I,V} &= \left(h_{I,V}^{\mathrm{tree}} + h_{I,V}^{(1/m^2)}\right) + h_{I,V}^{(1,0)} + h_{I,V}^{(0,1)} + h_{I,V}^{(1,1)}\,, \\ h_{I,A} &= h_{I,A}^{\mathrm{tree}} + h_{I,A}^{(0,1)}\,, \end{aligned} \tag{2.7}$$

where the $h_{I,F}^{\mathrm{tree}}$ and $h_{I,V}^{(1/m^2)}$ (due to the $j_V^{(1/m^2)}$) are the tree-level contributions, and $h_{I,F}^{(i,j)}$ incorporate the contributions from radiative corrections (the superscript (i,j) denotes the

[4] The only missing constant in ref. [18] is related to the three-loop static potential where recently the fermion corrections became available [19].

[5] We include the effect due to $j_V^{(1/m^2)}$ with $d_v^{\mathrm{tree}} = 1$ into $h_{I,V}^{(1/m^2)}$ for convenience, see eq. (2.7).

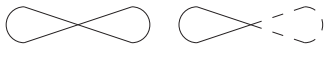

Figure 2: Two-line MIs. The solid and dashed lines correspond to propagators with mass m_t and M_W, respectively.

electroweak- and QCD-loop order, respectively). As one can see from the expression of the axial-vector current j_A, H_A is suppressed by $\vec{D}^{\,2}/m_t^2 \sim E/m_t$. Thus one-loop QCD corrections to $h_{I,A}$ correspond to NNNLO effects. In section 4 we will provide explicit results for $h_{I,V}^{(1,0)}$ and $h_{I,V}^{(1,1)}$ induced by the exchange of a photon.

Hard QCD corrections to the $\gamma t\bar{t}$ and $Zt\bar{t}$ vertices modify the matching coefficients c_v and c_a at loop level. We absorb these effects into helicity amplitudes and obtain (using $h_{I,V}^{(1/m^2)} = -h_{I,V}^{\rm tree}\, E/(6m_t)$)

$$h_{I,V}^{(0,1)} = \left(c_v^{(1)} - \frac{E\, d_v^{(1)}}{6m_t}\right) h_{I,V}^{\rm tree}\,, \qquad h_{I,A}^{(0,1)} = c_a^{(1)}\, h_{I,A}^{\rm tree}\,, \tag{2.8}$$

with $c_v^{(\rm i)}$, $d_v^{(\rm i)}$ being the i-loop contribution to the matching coefficients. For the purpose of this paper only the one-loop contribution $c_v^{(1)}$ is needed (see below for explicit expressions). Let us mention that the two-loop QCD corrections have been evaluated in refs. [27, 28] and the three-loop corrections induced by a light quark loop in ref. [29].

3. Technical details of the two-loop calculation

Let us in this section provide some technical details about the evaluation of the two-loop diagrams. They are generated with QGRAF [30] and further processed with q2e and exp [31, 32]. The reduction of the integrals is performed with the program crusher [33] which implements the Laporta algorithm [34, 35]. We arrive at 29 master integrals (MI) which are depicted in figures 2–5. All diagrams occur with the propagators raised to power one. Note that there are two more MIs of type 3.10: one with a squared top quark propagator and one with a squared massless propagator. Similarly, an additional MI arises from type 3.11 with a squared massless propagator.

We refrain from presenting the explicit results for all MIs in this paper but provide them in form of a Mathematica file[6] MIttewW.m using the conventions as defined in eq. (A.3) which corresponds to the one-loop tadpole integral. In all results presented in this file a factor $\left(\mu^2/m_t^2\right)^{2\epsilon}$ with $d = 4 - 2\epsilon$ has to be multiplied.

Some MIs factorize into one-loop integrals or contain only one dimensionful scale. Most of these integrals are available in the literature and can, e.g., be found in refs. [36 – 39, 10, 40].

As we will see in section 4 a rapid convergence is observed if one considers an expansion of the matching coefficient in the quantity $z = M_W^2/m_t^2$. For this reason we evaluate the

[6]The file is available from http://www-ttp.particle.uni-karlsruhe.de/Progdata/ttp08/ttp08-43.

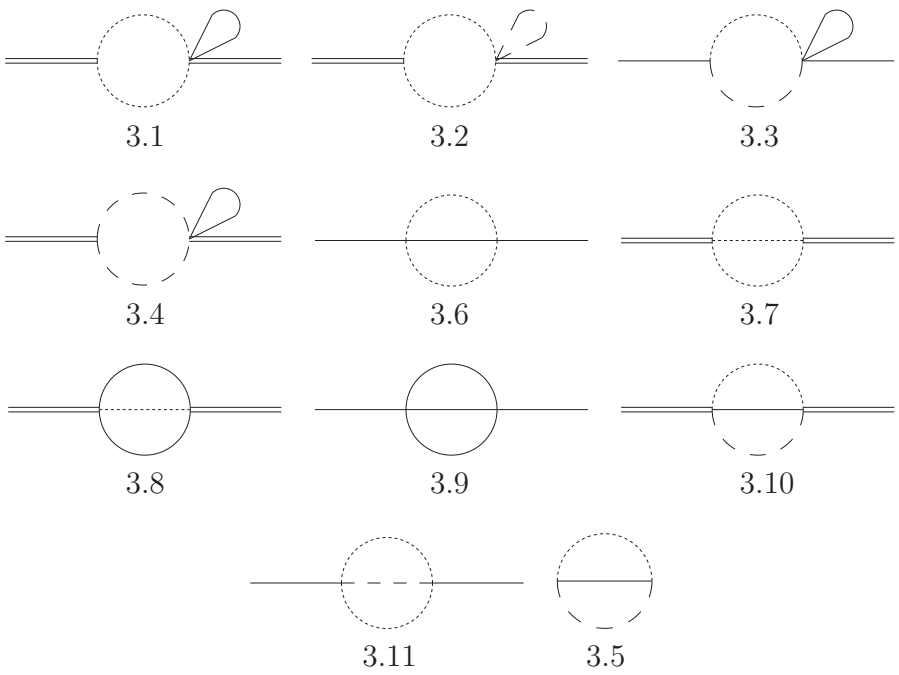

Figure 3: Three-line MIs. The solid, dashed and dotted lines correspond to propagators with mass m_t, M_W and 0, respectively. Single external lines are on the mass shell with mass m_t whereas double external line have mass $2m_t$. The topology denoted by 3.10 contains three master integrals, topology 3.11 contains two MIs.

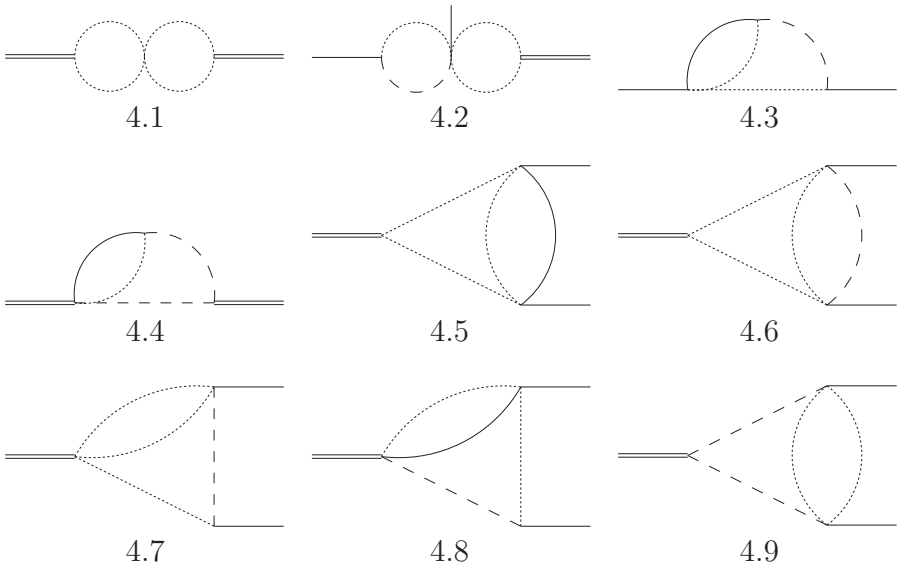

Figure 4: Four-line MIs. For the notation we refer to figure 3.

two-scale MIs in this limit. A promising method is based on differential equations (see ref. [41] for a recent review) which provide the expansion in an automatic way once the initial conditions are specified. Let us as an example consider the five-line integral MI(5.2)

JHEP01(2009)038

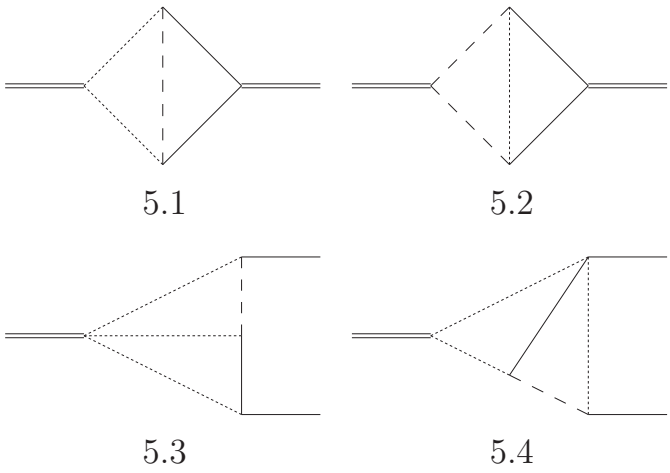

Figure 5: Five-line MIs. For the notation we refer to figure 3.

(cf. figure 5) which fulfills the following differential equation

$$\begin{aligned}\frac{\mathrm{d}}{\mathrm{d}z}\,\mathrm{MI}(5.2) = {} & \frac{d-4}{z-1}\,\mathrm{MI}(5.2) + \frac{3(z-2)(d-2)^2}{16m_t^6(d-3)(z-4)(z-1)^2 z}\,\mathrm{MI}(2.2) \\ & - \frac{(d-2)}{4m_t^4(z-1)^2}\,\mathrm{MI}(3.4) - \frac{(d-2)}{8m_t^4(z-1)^2}\,\mathrm{MI}(3.5) \\ & + \frac{(3d-8)(z-6)}{16m_t^4(z-4)(z-1)z}\,\mathrm{MI}(3.10) \\ & + \frac{(d-4)(z-9)(z+2)}{16m_t^2(d-3)(z-4)(z-1)z}\,\mathrm{MI}(3.10.1) \\ & - \frac{\left(z^2-z+6\right)}{4m_t^2(z-4)(z-1)^2 z}\,\mathrm{MI}(3.10.2) + \frac{(d-3)}{2m_t^2(z-1)^2}\,\mathrm{MI}(4.4)\,. \end{aligned} \tag{3.1}$$

MI(3.10.1) and MI(3.10.2) denote the MIs of the type 3.10 with a squared massless and top quark propagator, respectively. In order to solve this equation it is necessary to know the results of all integrals with less than five lines. With the help of the ansatz

$$\mathrm{MI}(5.2) = \sum c_{ijk}\,\epsilon^i z^j (\ln z)^k\,, \tag{3.2}$$

the differential equation can be expanded in ϵ and z. As a result it reduces to algebraic equations for the coefficients c_{ijk}. In every order in ϵ there is one constant c_{ijk} which can not be determined with this procedure. It is obtained from the initial condition at $z = 0$, which in the case of MI(5.2) can be found in ref. [36]. In this way we have computed expansion terms up to order z^{10} which can be found in the Mathematica file mentioned

above. For illustration we present the first two expansion terms of MI(5.2) which read

$$\begin{aligned}
\mathrm{MI}(5.2)m_t^2 \;=\; & \frac{1}{4}\pi^2\ln 2 - 2\ln^3 2 - \frac{1}{3}\pi^2\ln 3 + 2\ln^2 2\ln 3 - \ln 2\ln^2 3 + \frac{\ln^3 3}{3} \\
& - \mathrm{Li}_3(-2) + \frac{1}{2}\mathrm{Li}_3\left(\frac{1}{4}\right) - 2\mathrm{Li}_3\left(\frac{2}{3}\right) + \mathrm{Li}_3\left(\frac{3}{4}\right) + \frac{21\zeta(3)}{8} \\
& - i\pi\left(\frac{\pi^2}{12} + \frac{1}{2}\ln^2 2\right) - z\Bigg[i\pi\left(\frac{1}{2} - \frac{1}{4}\ln 2 + \frac{3}{4}\ln 3 - \frac{3}{8}\ln z\right) \\
& + \frac{3}{8}\ln 3\ln z - \frac{3\ln^2 3}{8} + \frac{1}{4}\ln 2\ln 3 - \frac{\ln^2 2}{4} - \ln 2 \\
& + \frac{17\pi^2}{48} - \frac{1}{8}\mathrm{Li}_2\left(\frac{3}{4}\right)\Bigg] + \mathcal{O}(z^2)\,. \qquad (3.3)
\end{aligned}$$

Note that for some integrals the differential equation can be solved with the help of Harmonic Polylogarithms [42] which immediately leads to a closed result.

It is interesting to mention that for the integrals MI(4.3) and MI(4.4) no initial condition is needed in order to obtain all the coefficients in the ansatz. They are completely fixed by the corresponding differential equation and the solutions for the integrals of the subtopologies. For all other integrals initial conditions at $z = 0$ are required. As already mentioned above most of them can be found in the literature or are quite simple to compute using standard techniques. However, we could not get analytic results for five[7] coefficients in the ϵ-expansion of the integrals MI(4.5), MI(4.8), MI(5.3) and MI(5.4) at $z = 0$. We calculated these coefficients using the Mellin-Barnes method (see, e.g., Ref [43]) where we used the program packages AMBRE [44] and MB [45].

The Mellin-Barnes representation for a given integral is not unique. In particular it might happen that the convergence of the resulting numerical integration turns out to be good in one case whereas a poor convergence is observed in other cases. The crucial quantity in this respect is the asymptotic behaviour of the Γ function for large imaginary part which is given by

$$\Gamma(a \pm ib) \overset{b\to\infty}{\simeq} \sqrt{2\pi}e^{\pm i\frac{\pi}{4}(2a-1)}e^{\pm ib(\ln b - 1)}e^{-\frac{b\pi}{2}}b^{a-\frac{1}{2}}\,, \qquad (3.4)$$

where the first two exponential factors lead to oscillations. Let us discuss this in more detail for the Mellin-Barnes representation of the integral MI(4.5)

$$\begin{aligned}
\mathrm{MI}(4.5) \;=\; & \left(\frac{e^{\gamma_E}\mu^2}{m_t^2}\right)^{2\epsilon}\int_{-i\infty}^{+i\infty}\frac{dz_1}{2\pi i}\int_{-i\infty}^{+i\infty}\frac{dz_2}{2\pi i}\,e^{i\pi(2\epsilon+z_1)}4^{-2\epsilon-z_2} \\
& \times\frac{\Gamma(1-\epsilon)\Gamma(-\epsilon-z_1+1)\Gamma(-z_1)\left[\Gamma(-2\epsilon-z_2+1)\right]^2}{\Gamma(-3\epsilon-z_1+2)\Gamma(-2\epsilon-z_1+2)\Gamma(-4\epsilon-2z_2+2)} \\
& \times\Gamma(-4\epsilon-z_1-z_2+2)\Gamma(z_1-z_2)\Gamma(\epsilon+z_2)\Gamma(2\epsilon+z_2)\,, \qquad (3.5)
\end{aligned}$$

where $\gamma_E = 0.577216\ldots$ and the contour of integration is chosen in such a way that the poles of the Γ functions with $+z_i$ are separated from the poles of the Γ functions with

[7] One more coefficient can be obtained analytically from the requirement that our final result is finite. It agrees perfectly with our numerical result.

JHEP01(2009)038

$-z_i$. Using the package MB we can expand the integrand in ϵ. For the finite contribution this leads to a sum of an analytic part, a one-dimensional Mellin-Barnes integral and a two-dimensional one. The latter correspond to the integral in eq. (3.5) for $\epsilon = 0$. If we insert in this expression the asymptotic behaviour for the Γ functions as given in eq. (3.4) one can see that the integrand of the two-dimensional integral falls off exponentially, except for $\mathrm{Im}(z_2) = 0, \mathrm{Im}(z_1) < 0$.[8] On this line the drop-off only shows a power-law behaviour which is dictated by the last factor of eq. (3.4). In our particular case the drop-off turns out to be extremely slow for the integration contour chosen by MB which corresponds to $\mathrm{Re}(z_1) = -1/4$ and $\mathrm{Re}(z_2) = -1/2$. Thus it is hard to get an accurate result by the numerical integration since a highly oscillating functions has to be integrated. A closer look to the fall-off behaviour in eq. (3.4) shows that it is possible to improve the drop-off for $\mathrm{Im}(z_1) \to -\infty$ by taking residues of the integrand in z_2 and thus shifting the integration contour for z_2 more and more to positive values for $\mathrm{Re}(z_2)$. In this way the integrand becomes well-behaved and can be integrated numerically with sufficiently high precision.

It has already been pointed out in [45] that for certain kinematical configurations the Mellin-Barnes integrals exhibit poor convergence behaviour. We have shown that at least for the threshold integrals needed in our calculation, it is possible to choose the integration paths in a way to make the numerical integration possible. One may hope that with the approach described here it will turn out to be possible to use Mellin-Barnes integration for other troublesome integrals, too.

Let us mention that in the case of MI(4.5) there is an alternative possibility to improve the numerical properties of the eq. (3.5): after the variable transformation $z_2 \to z_2 - 2\epsilon$ MB chooses integration contours which lead to a rapid convergence of the numerical integration. We have checked that both approaches lead to the same results and obtained 9 digits for the finite part of MI(4.5) in eleven minutes of CPU time.

The remaining three integrals show similar properties as MI(4.5). In all cases it is possible to end up with integrals which could be integrated numerically. Our results read

$$\begin{aligned}
\mathrm{MI}(4.5) &= \left(\frac{\mu^2}{m_t^2}\right)^{2\epsilon} \left[\frac{1}{2\epsilon^2} + \frac{1}{\epsilon}\left(\frac{5}{2} - 2\ln 2 + i\pi\right) - 4.81543683(7)\right. \\
&\quad \left. + 4i\pi(1 - \ln 2)\right], \\
\mathrm{MI}(4.8)|_{z=0} &= \left(\frac{\mu^2}{m_t^2}\right)^{2\epsilon} \left[\frac{1}{2\epsilon^2} + \frac{1}{\epsilon}\left(\frac{5}{2} + i\pi\right) + \frac{19}{2} - \frac{23\pi^2}{24} - \frac{5\ln^2 2}{2} - \frac{3\ln 3}{2}\right. \\
&\quad + \frac{5}{2}\ln 2 \ln 3 - \frac{5}{4}\mathrm{Li}_2\left(\frac{3}{4}\right) + \frac{i\pi}{2}(11 - 5\ln 2) - \epsilon\, 16.690539(1) \\
&\quad - i\pi\epsilon\left(- \frac{45}{2} + \frac{35\pi^2}{24} + 3\ln 2 - \frac{21\ln^2 2}{4} + 6\ln 3 + 2\mathrm{Li}_2(-2)\right. \\
&\quad \left.\left. - 4\mathrm{Li}_2\left(\frac{1}{4}\right)\right)\right],
\end{aligned}$$

[8] Note that for these values of z_1 the exponential factor in the integrand of (3.5) increases exponentially.

$$m_t^2\,\mathrm{MI}(5.3)|_{z=0} = 2.704628(4) - 5.167709(4)i\,,$$
$$m_t^2\,\mathrm{MI}(5.4)|_{z=0} = 2.70543(6) - 1.91431(6)i\,. \tag{3.6}$$

The accuracy for the finite part of these integrals is sufficient to obtain the final result with four significant digits.

Note that contrary to the default settings of MB we do not use Vegas for the multi-dimensional numerical integrations. Instead we use Divonne which is available from the Cuba library [46]. For the integrals we have considered it leads to more accurate results using less CPU time.

We have performed an independent check of the initial conditions for all the MIs employing the method of sector decomposition. In particular we used the program FIESTA [47].

4. The $\gamma t\bar{t}$ vertex

In this section we discuss $\mathcal{O}(\alpha\alpha_s)$ corrections to the $\gamma t\bar{t}$ vertex due to W boson and gluon exchanges with incoming photon momentum at $q^2 = 4m_t^2$, the production threshold of top quark pairs. This leads to corrections to $h_{I,V}^{(1,1)}$ mediated by a virtual photon, i.e., to the first term of $h_{I,V}^{\mathrm{tree}}$ in eq. (2.5). We denote by Γ_A^t the contribution of the sum of all one-particle-irreducible diagrams to the $\gamma t\bar{t}$ vertex and parameterize the radiative corrections in the form

$$\hat{\Gamma}_A^t = Q_t + \hat{\Gamma}_A^{t,(0,1)} + \hat{\Gamma}_A^{t,(1,0)} + \hat{\Gamma}_A^{t,(1,1)}\,, \tag{4.1}$$

where the hat denotes renormalized quantities. Substituting $\hat{\Gamma}_A^t$ for the Q_t in first line of eq. (2.5) and retaining the relevant orders in the electroweak and strong couplings leads to the corrections to the helicity amplitudes, $h_{I,V}^{(0,1)}, h_{I,V}^{(1,0)}$ and $h_{I,V}^{(1,1)}$. We further decompose $\hat{\Gamma}_A^t$ (and similarly the quantities on the right-hand side of eq. (4.1)) according to the contributions from the Higgs, Z and W boson exchanges:

$$\hat{\Gamma}_A^t = \hat{\Gamma}_{A,H}^t + \hat{\Gamma}_{A,Z}^t + \hat{\Gamma}_{A,W}^t\,. \tag{4.2}$$

In this paper we compute the corrections up to order $\alpha\alpha_s$ to $\hat{\Gamma}_{A,W}^t$. The other two quantities have been computed in ref. [10] where the matching coefficients $c_v^{\mathrm{H,mix}}$ and $c_v^{\mathrm{Z,mix}}$ have been introduced. We have the following relations

$$\hat{\Gamma}_{A,H}^{t,(1,1)} = \frac{\alpha\alpha_s}{\pi^2 s_w^2}\,Q_t C_F\,c_v^{\mathrm{H,mix}}, \qquad \hat{\Gamma}_{A,Z}^{t,(1,1)} = \frac{\alpha\,\alpha_s}{\pi^2 s_w^2}\,Q_t C_F\,c_v^{\mathrm{Z,mix}}\,. \tag{4.3}$$

In our calculation we adapt in the electroweak sector the 't Hooft-Feynman gauge, i.e. $\xi_W = 1$, which guarantees a simple form of the W boson propagator. Note that $\xi_W \neq 1$ introduces an additional mass scale in our calculation which would lead to significantly more complicated integrals at two-loop order. We want to mention that our final result depends on ξ_W. This dependence only cancels out after including the self-energy and box contributions. There is no gauge parameter dependence in $\hat{\Gamma}_{A,H}^t$ which only occurs in the

vertex and self-energy contributions. Also the vertex corrections involving the Z boson ($\hat{\Gamma}^{t}_{A,Z}$) are independent of the corresponding gauge parameter.

Although the one-loop results are well-known, we start our discussion from this order since they enter the renormalization of the two-loop expressions.

4.1 One-loop corrections

The renormalized QCD contribution is given by

$$\hat{\Gamma}^{t,(0,1)}_{A} = \Gamma^{t,(0,1)}_{A} + Q_t\, Z_2^{(0,1)}\,, \tag{4.4}$$

where Z_2 is the on-shell wave function renormalization for external top quarks. The expressions on the right-hand side of eq. (4.4) are given by

$$\begin{aligned}
\Gamma^{t,(0,1)}_{A} &= Q_t\, \frac{\alpha_s C_F}{4\pi} \left(\frac{\mu^2}{m_t^2}\right)^{\epsilon} \left[\frac{3}{\epsilon} - 4 + \epsilon\left(8 + \frac{\pi^2}{4}\right)\right], \\
Z_2^{(0,1)} &= \frac{\alpha_s C_F}{4\pi} \left(\frac{\mu^2}{m_t^2}\right)^{\epsilon} \left[-\frac{3}{\epsilon} - 4 - \epsilon\left(8 + \frac{\pi^2}{4}\right)\right],
\end{aligned} \tag{4.5}$$

where $C_F = 4/3$. In eq. (4.5) the $\mathcal{O}(\epsilon)$ terms are kept since they enter the finite part of the two-loop expression. For the renormalized vertex we have the relation

$$\hat{\Gamma}^{t,(0,1)}_{A} = Q_t\, c_v^{(1)} = -8\, Q_t\, \frac{\alpha_s C_F}{4\pi}\,(1 + \epsilon\, L_\mu) + \mathcal{O}(\epsilon^2)\,, \tag{4.6}$$

where $L_\mu = \ln \frac{\mu^2}{m_t^2}$. The one-loop formula for the electroweak corrections is given by

$$\hat{\Gamma}^{t,(1,0)}_{A} = \Gamma^{t,(1,0)}_{A} + Q_t\, Z_2^{(1,0)} + T_t^3\, Z_{\rm CT}^{(1,0)}\,, \tag{4.7}$$

where $Z_{\rm CT}^{(1,0)}$ is a counterterm associated with Z-photon mixing at zero-momentum transfer [48] which reads

$$Z_{\rm CT}^{(1,0)} = \frac{\alpha}{4\pi s_w^2}\left(-\frac{1}{\epsilon} - \ln\frac{\mu^2}{M_W^2}\right) + \mathcal{O}(\epsilon)\,. \tag{4.8}$$

As we will see later the $\mathcal{O}(\epsilon)$ term for $Z_{\rm CT}^{(1,0)}$ is not needed. We present the remaining two ingredients as a series expansion of $z = M_W^2/m_t^2$, the exact formulae are collected in the appendix for convenience. The results for $Z_{2,W}^{(1,0)}$ reads

$$\begin{aligned}
Z_{2,W}^{(1,0)} = \frac{\alpha}{4\pi s_w^2}\left(\frac{\mu^2}{m_t^2}\right)^{\epsilon} \Bigg\{ & -\frac{1}{\epsilon}\left(\frac{1}{4} + \frac{1}{8z}\right) - \frac{i\pi}{8z} - \frac{L_z}{4} - \frac{i\pi}{2} - \frac{1}{4} - \left(\frac{L_z}{8} + \frac{i\pi}{8} + \frac{21}{16}\right) z \\
& + \epsilon\left[\frac{7\pi^2}{96z} + \frac{L_z^2}{8} - \frac{L_z}{4} + \frac{5\pi^2}{16} - \frac{i\pi}{2} - \frac{3}{4} + \left(\frac{L_z^2}{16} + \frac{3L_z}{16} + \frac{\pi^2}{12} - \frac{9i\pi}{8} - \frac{27}{32}\right) z\right]\Bigg\} \\
& + \mathcal{O}(z^2)\,,
\end{aligned} \tag{4.9}$$

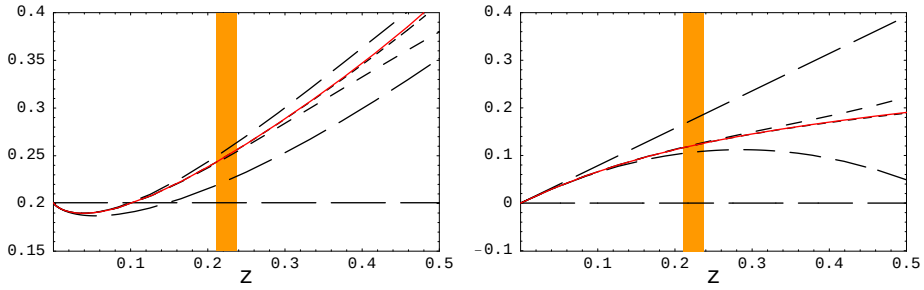

Figure 6: Electroweak one-loop corrections to the photon vertex $\hat{\Gamma}^{t,(1,0)}_{A,W}$ normalized to $\alpha/(4\pi s_w^2)/z$ as a function of $z = M_W^2/m_t^2$, for real part (left panel) and imaginary part (right panel), respectively. The (black) dashed lines include successively higher orders in z starting from z^0 (long dashes) to z^4 (short dashes) and the (red) solid line is the exact one-loop correction. The (orange) band marks the physical range of $z = (80.40\,\mathrm{GeV}/m_t)^2$ varying the top quark mass between 165 and 175 GeV.

and $\Gamma^{t,(1,0)}_{A,W}$ is given by

$$
\begin{aligned}
\Gamma^{t,(1,0)}_{A,W} = {} & \frac{\alpha}{4\pi s_w^2} Q_b \left(\frac{\mu^2}{m_t^2}\right)^{\epsilon} \left\{ \frac{1}{\epsilon}\left(\frac{1}{8z}+\frac{1}{4}\right) + \frac{1}{z}\left(\frac{i\pi}{8} - \frac{2\ln 2}{3} + \frac{1}{6}\right) \right. \\
& + \frac{L_z}{4} + \frac{i\,\pi}{2} - \frac{1}{12} - \frac{2\ln 2}{3} + \left(\frac{L_z}{8} + \frac{i\,\pi}{8} + \frac{2\ln 2}{3} + \frac{7}{48}\right) z \\
& + \epsilon \left[-\frac{1}{z}\left(\frac{7\pi^2}{96} + \frac{i\pi\big(4\ln 2 - 1\big)}{6} - \frac{2\ln 2\big(3\ln 2 - 5\big)}{9} - \frac{5}{18}\right) \right. \\
& - \frac{L_z^2}{8} + \frac{L_z}{4} - \frac{5\pi^2}{16} - \frac{i\pi\big(4\ln 2 - 1\big)}{6} + \frac{2\ln 2\,\big(3\ln 2 + 1\big)}{9} + \frac{7}{36} \\
& \left. \left. - \left(\frac{L_z^2}{16} + \frac{3L_z}{16} + \frac{2\ln 2\big(3\ln 2 + 1\big)}{9} + \frac{\pi^2}{12} - \frac{i\pi\big(16\ln 2 - 1\big)}{24} - \frac{115}{288}\right) z \right] \right\} \\
& + \frac{\alpha}{4\pi s_w^2} T_t^3 \left(\frac{\mu^2}{m_t^2}\right)^{\epsilon} \left\{ \frac{1}{\epsilon}\left(\frac{1}{4z}+\frac{3}{2}\right) + \frac{1}{z}\left(\frac{i\pi}{4} - \frac{2\ln 2}{3} + \frac{2}{3}\right) \right. \\
& + \frac{3i\pi}{2} - 3\ln 2 + 3 - \left(\frac{5L_z}{8} - \frac{15}{16} + \frac{5i\pi}{8} - \frac{7\ln 2}{4}\right) z \\
& + \epsilon \left[-\frac{1}{z}\left(\frac{7\pi^2}{48} + \frac{2i\pi\big(\ln 2 - 1\big)}{3} - \frac{2\ln 2\big(3\ln 2 - 8\big)}{9} - \frac{13}{9}\right) \right. \\
& - \frac{7\pi^2}{8} - 3i\pi\big(\ln 2 - 1\big) + 3\ln 2\big(\ln 2 - 2\big) + 6 \\
& \left. \left. + \left(\frac{5L_z^2}{16} - \frac{11L_z}{16} + \frac{5\pi^2}{12} + \frac{i\pi\big(7\ln 2 + 1\big)}{4} - \frac{7\ln^2 2}{4} + \frac{39}{32}\right) z \right] \right\} \\
& + \mathcal{O}(z^2)\,,
\end{aligned}
\tag{4.10}
$$

where $L_z = \ln z$ and $\alpha = e^2/(4\pi)$ is the fine-structure constant in the Thomson limit. Again the $\mathcal{O}(\epsilon)$ terms are retained due to their relevance for the two-loop renormalization. Note that we keep the imaginary parts of both $\Gamma^{t,(0,1)}_{A,W}$ and $Z^{(0,1)}_{2,W}$. See appendix B for more details. At one-loop order this only affects the finite part; at two loops also the pole parts are concerned (see below).

JHEP01(2009)038

We refrain from listing an analytical result for $\hat{\Gamma}_A^{t,(1,0)}$ but compare in figure 6 the approximated result to the exact one. The latter is represented by the (red) solid line whereas the dashed lines correspond to the expansions including successively higher orders in z. As one can see, the expression including the correction of order z^3 provides at the physical point $z \approx 0.23$ a perfect approximation to the exact result far below the per cent level. The approximated results are based on the following expressions

$$\begin{aligned}
\hat{\Gamma}_{A,W}^{t,(1,0)} &= \frac{\alpha}{4\pi s_w^2}\Bigg[\frac{0.20}{z} + \big(0.48 + 0.79\,i + 0.25\ln z\big) \\
&\quad + z\,\big(-0.0024 - 1.37\,i - 0.44\,\ln z\big) + z^2\,\big(-0.072 + 1.39\,i + 0.44\,\ln z\big) \\
&\quad + z^3\,\big(0.34 - 0.53\,i - 0.17\,\ln z\big) + z^4\,\big(0.13 + 0.23\,i + 0.074\,\ln z\big)\Bigg] \\
&\quad + \mathcal{O}(z^5) \\
&= \Bigg[2.48_{1/z} + 0.25_1 + 0.39_z - 0.095_{z^2} + 0.017_{z^3} + 0.00013_{z^4} \\
&\quad + i\,\big(2.11_1 - 0.80_z + 0.18_{z^2} - 0.015_{z^3} + 0.0014_{z^4}\big)\Bigg] \times 10^{-3}\,, \qquad (4.11)
\end{aligned}$$

where the subscript in the last line indicate their order in the z expansion and for the input parameters the following values have been used [49, 50]

$$\begin{aligned}
\alpha_s &= 0.108\,, \qquad \alpha(M_Z) = 1/128.9\,, \qquad s_w^2 = 0.23\,, \\
M_W &= 80.40\,\text{GeV}\,, \qquad m_t = 172.4\,\text{GeV}\,. \qquad (4.12)
\end{aligned}$$

Note that in our numerical analysis we use α at high energy scale.[9]

The corrections in eq. (4.11) are dominated by the leading terms proportional to m_t^2/M_W^2. One observes a rapid convergence, so that the term of order z^3 can safely be neglected. Inserting the results in eq. (4.1) the overall size of the electroweak corrections (from the diagrams involving a W boson) amounts to about 0.5% and is unusually small. For comparison, we note that $\hat{\Gamma}_{A,Z}^{t,(1,0)}$ and $\hat{\Gamma}_{A,H}^{t,(1,0)}$ lead to corrections of 0.3% and 3.2% (for $M_H = 120\,\text{GeV}$), respectively. Let us mention that the one-loop QCD corrections provides a contribution "-61×10^{-3}" to the last line of eq. (4.11) thus resulting in a 9% correction.

From eq. (4.11) one obtains the corresponding corrections to the helicity amplitude as

$$\Big[h_{I,V}^{(1,0)}\Big]_{A,W} = Q_e \hat{\Gamma}_{A,W}^{t,(1,0)}\,, \qquad (4.13)$$

which immediately leads to the correction to the cross section with the help of eq. (2.1). Taking at tree-level both the photon and Z exchange diagram we obtain a shift of 0.9% to $R(e^+e^- \to t\bar{t}X)$ due to the W boson contribution to $\gamma t\bar{t}$ vertex at one-loop.

4.2 Two-loop order $\alpha\alpha_s$ renormalization

The renormalized $\gamma t\bar{t}$ vertex at order $\alpha\alpha_s$ is given by

$$\begin{aligned}
\hat{\Gamma}_A^{t,(1,1)} &= \Gamma_A^{t,(1,1)} + T_t^3\, Z_{\text{CT}}^{(1,1)} + Q_t\, Z_2^{(1,1)} \\
&\quad + \Big(Z_2^{(1,0)}\,\Gamma_A^{t,(0,1)} + Z_2^{(0,1)}\,\Gamma_A^{t,(1,0)}\Big) + \frac{T_t^3}{Q_t}\, Z_{\text{CT}}^{(1,0)}\,\hat{\Gamma}_A^{t,(0,1)}\,, \qquad (4.14)
\end{aligned}$$

[9] This is theoretically preferable because it is devoid of non-perturbative hadronic effects.

where the first line corresponds to genuine two-loop diagrams and the second line consists of products of one-loop diagrams. For the latter we already listed all the relevant expressions in the previous Subsection. Note that in the last term the renormalized one-loop vertex appears and thus the $\mathcal{O}(\epsilon)$ term for $Z_{\rm CT}^{(1,0)}$ is not needed.

Formula (4.14) takes only care of the renormalization of the external lines and the electric charge which means that the un-renormalized two-loop quantities in the first line are understood as the sum of the amputated two-loop diagrams and the corresponding counterterm diagrams for the top quark mass and the top quark Yukawa coupling. The latter are renormalized in the on-shell scheme.

It is easy to see that for the two-loop counterterm we have $Z_{\rm CT}^{(1,1)} = 0$ since at one-loop order only bosonic and no fermionic diagrams contribute. The two-loop on-shell wave function factor $Z_2^{(1,1)}$ has been computed in ref. [51]. We confirmed the result by an independent calculation and added the imaginary part which is necessary in our framework. The result reads

$$
\begin{aligned}
Z_{2,W}^{(1,1)} = {} & \frac{\alpha}{4\pi s_w^2}\frac{\alpha_s C_F}{4\pi}\left\{\frac{1}{\epsilon^2}\left(\frac{3}{4}+\frac{3}{4z}\right)+\frac{1}{\epsilon}\left[\frac{1}{z}\left(\frac{3L_\mu}{2}+\frac{7}{4}+\frac{3i\pi}{8}\right)+\frac{3L_\mu}{2}+\frac{3L_z}{4}\right.\right. \\
& +\frac{17}{8}+\frac{3i\pi}{2}+\left(\frac{3L_z}{8}+\frac{63}{16}+\frac{3i\pi}{8}\right)z-\left(\frac{9\ln z}{4}-\frac{5}{4}+\frac{9i\pi}{4}\right)z^2\Big] \\
& +\frac{1}{z}\left(\frac{3L_\mu^2}{2}+\frac{(14+3i\pi)L_\mu}{4}+\frac{3\zeta(3)}{2}-\frac{i\pi^3}{6}-\frac{\pi^2}{4}+\frac{27i\pi}{8}+\frac{79}{16}\right) \\
& +\frac{3L_\mu^2}{2}+\left(\frac{3L_z}{2}+\frac{17}{4}+3i\pi\right)L_\mu-\frac{3L_z^2}{8}+\frac{7L_z}{4}-3\zeta(3)+\frac{i\pi^3}{3}-\frac{\pi^2}{8} \\
& +\frac{3i\pi}{2}-\frac{3}{16}+\left[\left(\frac{3L_z}{4}+\frac{3i\pi}{4}+\frac{63}{8}\right)L_\mu-\frac{3L_z^2}{16}-\frac{(1+28i\pi)L_z}{16}\right. \\
& \left.-\frac{15\zeta(3)}{2}+\frac{5i\pi^3}{6}+\frac{5\pi^2}{6}-\frac{121i\pi}{24}+\frac{661}{32}\right]z+\left[\left(-\frac{9L_z}{2}+\frac{5}{2}-\frac{9i\pi}{2}\right)L_\mu\right. \\
& \left.\left.+\frac{9L_z^2}{8}+\left(\frac{1}{2}-\frac{5i\pi}{6}\right)L_z-\frac{317}{48}+\frac{547i\pi}{72}+\frac{79\pi^2}{36}-i\pi^3+9\zeta(3)\right]z^2\right\} \\
& +\mathcal{O}(z^3)\,, \qquad (4.15)
\end{aligned}
$$

where terms up to order z^2 have been included ($\zeta(3) = 1.20205\cdots$).

In the following we provide the result for the un-renormalized vertex corrections where the finite part is given in numerical form. Our result reads

$$
\begin{aligned}
\Gamma_{A,W}^{t,(1,1)} = {} & \frac{\alpha}{4\pi s_w^2}\frac{\alpha_s C_F}{4\pi}\left\{\frac{2}{\epsilon^2}+\frac{1}{\epsilon}\left[-\frac{1}{z}\left(\frac{1}{3}-\frac{i\pi}{4}+\frac{\ln 2}{3}\right)+4L_\mu-\frac{L_z}{4}+\frac{7i\pi}{4}+\frac{5}{3}-\frac{23\ln 2}{6}\right.\right. \\
& \left.-z\left(\frac{17L_z}{16}-\frac{47\ln 2}{24}+\frac{17i\pi}{16}-\frac{121}{96}\right)-z^2\left(\frac{17L_z}{96}+\frac{185}{576}+\frac{17i\pi}{96}-\frac{65\ln 2}{48}\right)\right] \\
& +\frac{1}{z}\Big(\big[-2.66-3.79\big]-L_\mu\big[1.13-1.57i\big]\Big)+4.00\,L_\mu^2 \\
& +L_\mu\big(-0.50L_Z-\big[1.98-11.00i\big]\big)+0.13L_z^2+0.08L_z+\big[10.03-23.63i\big] \\
& +z\left[L_\mu\Big(\big[5.24-6.68i\big]-2.13\,L_z\Big)+0.53\,L_z^2-L_z\big[0.77-7.76i\big]\right.
\end{aligned}
$$

$$-\big[11.84+5.62i\big]\Big]+z^2\left[L_\mu\Big(\big[1.23-1.11i\big]-0.35\,L_z\Big)\right.$$
$$\left.+0.09\,L_z^2-L_z\,\big[3.80+1.16i\big]+\big[9.31+18.63i\big]\right]\Big\}+\mathcal{O}(z^3)\,. \tag{4.16}$$

Let us mention that in our calculation we allowed for a general QCD gauge parameter ξ_S and used the independence of $\Gamma_A^{t,(1,1)}$ as a welcome check for the correctness of our result. Note that for the cancellation of ξ_S it is important to include the counterterm diagram for the top quark mass. The remaining ingredients in eq. (4.14) are individually ξ_S-independent. A further check of our calculation is based on a setup where we choose $M_W = 0$ from the very beginning. This leads to significantly simpler expressions during the reduction to master integral, which is completely independent from the one for finite M_W.

4.3 $\mathcal{O}(\alpha\alpha_s)$ corrections to the $\gamma t\bar{t}$ vertex

Inserting all ingredients into eq. (4.14) leads to

$$\begin{aligned}
\hat{\Gamma}_{A,W}^{t,(1,1)} &= \frac{\alpha}{4\pi s_w^2}\frac{\alpha_s C_F}{4\pi}\left[\frac{1}{z}\Big(-0.45-i\,2.06\Big)+\Big(6.34-i\,25.14-2.00\ln z\Big)\right.\\
&\quad +z\Big(-6.27-i\,6.10+\big(2.16+i\,4.10\big)\,\ln z\Big)\\
&\quad +z^2\Big(13.50-i\,31.29-\big(4.53+i\,2.91\big)\,\ln z\Big)\\
&\quad +z^3\Big(-41.06-i\,5.55+\big(0.59+i\,13.10\big)\,\ln z\Big)\\
&\quad \left.+z^4\Big(17.11-i\,9.99-\big(1.86+i\,5.36\big)\,\ln z\Big)\right]+\mathcal{O}(z^5)\\
&= \Big[\big(-0.64_{1/z}+2.89_1-0.64_z+0.30_{z^2}-0.13_{z^3}+0.014_{z^4}\big)\\
&\quad +i\big(-2.91_{1/z}-7.73_1-0.83_z-0.39_{z^2}-0.081_{z^3}-0.0013_{z^4}\big)\Big]\times 10^{-4}\,.
\end{aligned} \tag{4.17}$$

In figure 7 we show the result for $\hat{\Gamma}_A^{t,(1,1)}$ including first five terms of the z expansion. Taking the difference of two successive curves as a measure for the quality of the approximation we observe a rapid convergence at the physical point. Note that in contrast to the one-loop case the leading $1/z$ contribution is numerically not dominant.

In analogy to eq. (4.13) we obtain for the correction to the helicity amplitude

$$\Big[h_{I,V}^{(1,1)}\Big]_{A,W} = Q_e\hat{\Gamma}_{A,W}^{t,(1,1)}\,, \tag{4.18}$$

which results in a correction of 0.1% to R.[10]

[10]We did not take into account $\mathcal{O}(\alpha\alpha_s)$ interference terms, e.g., $\delta R \sim (8\pi/s)\left[2h_{I,V}^{(1,0)}h_{I,V}^{(0,1)}H_V\right]$. Such correction should be considered once the the two-loop box contributions are available.

JHEP01(2009)038

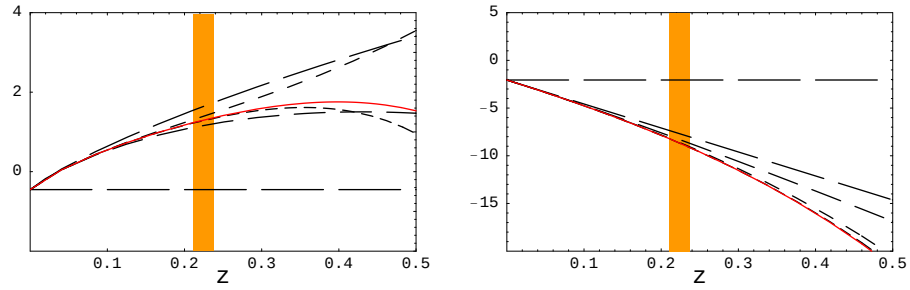

Figure 7: Electroweak two-loop correction to the photon vertex $\hat{\Gamma}^{t,(1,1)}_{A,W}$ normalized to $(\alpha_s \alpha C_F)/(16\pi^2 s_w^2)/z$ as a function of $z = M_W^2/m_t^2$, for real part (left panel) and imaginary part (right panel), respectively. The (black) long-dashed lines include successively higher orders in z starting from z^0 (long dashes) to z^4 (short dashes) and the orange band is the physical range of z (see figure 6).

Let us in the following briefly compare the new vertex corrections to the ones induced by a Higgs and Z boson. Note that the latter two contain a non-trivial scale dependence which is canceled by the corresponding contribution from the effective theory [10]. Choosing $\mu = m_t$ one obtains [8, 10]

$$\begin{aligned}
\hat{\Gamma}^{t,(1,0)}_{A,H} &= 21.1 \times 10^{-3}\,(10.6 \times 10^{-3}) \qquad \text{for} \quad M_H = 120\,(200)\,\text{GeV}\,, \\
\hat{\Gamma}^{t,(1,0)}_{A,W} &= 3.0 \times 10^{-3}\,, \\
\hat{\Gamma}^{t,(1,0)}_{A,Z} &= 1.7 \times 10^{-3}\,, \\
\hat{\Gamma}^{t,(1,1)}_{A,H} &= -17.6 \times 10^{-3}\,(-6.6 \times 10^{-3}) \qquad \text{for} \quad M_H = 120\,(200)\,\text{GeV}\,, \\
\hat{\Gamma}^{t,(1,1)}_{A,W} &= 0.2 \times 10^{-3}\,, \\
\hat{\Gamma}^{t,(1,1)}_{A,Z} &= -1.0 \times 10^{-3}\,.
\end{aligned} \tag{4.19}$$

One observes quite small corrections from the W and Z boson induced contributions. From eq. (4.19) one can read off that relatively big one-loop effects are obtained for light Higgs boson masses. However, there is a strong cancellation between the one- and two-loop terms resulting in corrections which have the same size as the sum of the one- and two-loop contributions of the W and Z boson diagrams. In general moderate effects are observed suggesting that in the electroweak sector perturbation theory works well, which is in contrast to the pure QCD corrections.

Let us at this point comment on the imaginary parts contained in eqs. (4.11) and (4.17) which are not taken into account in the numerical estimates for the corrections to R presented above. As we mentioned previously, "Im" in eq. (2.1) applies to the imaginary part which corresponds to the $t\bar{t}X$ final state or experimentally indistinguishable cuts involving bottom quarks and W bosons. Thus, it is necessary to separate imaginary parts arising from cutting, e.g., two W boson or two b quark lines from the $t\bar{t}X$ cuts in order to make a phenomenological prediction. This requires a dedicated analysis in the loop calculation, which is beyond the scope of this paper (see, e.g., ref. [13]).

JHEP01(2009)038

5. Conclusions and outlook

Mixed two-loop electroweak/QCD corrections to the $\gamma t\bar{t}$ vertex due to W boson and gluon exchange have been computed. The new contribution completes the order $\alpha\alpha_s$ corrections to the $\gamma t\bar{t}$ vertex. The numerical evaluation leads to a shift of 0.1% in the threshold production cross section of top quark pairs at e^+e^- colliders which is small as compared to the aimed 3% uncertainty for the theory predictions. Nevertheless, it is remarkable that in the sum of the order α and order $\alpha\alpha_s$ correction terms the sizeable one-loop contribution from the Higgs boson induced diagrams is screened resulting in numerical values comparable to the W and Z boson contributions.

We want to mention that the corrections evaluated in this paper, in particular the master integrals discussed in section 3, can be taken over in a straightforward way to the $Zt\bar{t}$ vertex containing a virtual W boson. However, for the $Zt\bar{t}$ vertex there is a further class of diagrams which has not been considered so far namely the one involving the ZZH vertex. This leads to a new mass configuration in the integrals which is not present for the photon-top quark vertex. Still, the techniques developed in section 3 are certainly quite useful for such a calculation. Note, that the axial-vector contribution is suppressed at threshold and thus one-loop corrections are sufficient. A further missing building block in order to complete the order $\alpha\alpha_s$ corrections to the process $e^+e^- \to t\bar{t}$ are the two-loop box diagrams. They are technically more involved and are thus postponed to future work.

Acknowledgments

We would like to thank J.H. Kühn for helpful discussions and A. Smirnov and M. Tentyukov for providing the package FIESTA prior to its publication. Y.K. thanks N. Zerf for comparing the electroweak one-loop corrections and Y. Sumino for discussions about the implementation of the sector decomposition method within Mathematica. D.S. acknowledges technical support by T. Hahn concerning to the Cuba library. This work is supported by the DFG Sonderforschungsbereich/Transregio 9 "Computergestützte Theoretische Teilchenphysik".

A. Exact result for $\Gamma^{t,(1,0)}_{A,W}$

Keeping the full dependence on ϵ the exact one-loop result for the $\gamma t\bar{t}$ vertex due to the W boson exchange reads (for massless bottom quarks)

$$\begin{aligned}\Gamma^{t,(1,0)}_{A,W} = \frac{\alpha}{4\pi s_w^2}\left(\frac{1}{-3+2\,\epsilon}\right)\Bigg[&\big(Q_b+2T_t^3\big)\big(1+2(1-\epsilon)z\big)\frac{A_0^{(\epsilon)}\big(M_W^2\big)}{8M_W^2}\\ &+\big(Q_b\,(5+z-4\epsilon)+2T_t^3\,(1+z)\big)\frac{(1-z)\big(1+2(1-\epsilon)z\big)}{8z(1+z)}B_0^{(\epsilon)}(m_t^2,M_W^2,0)\\ &-Q_b\frac{(1+2(1-\epsilon)z)(1-\epsilon)}{z(1+z)}B_0^{(\epsilon)}(4m_t^2,0,0)\\ &-T_t^3\left(\frac{1}{z}+5-4\epsilon\right)B_0^{(\epsilon)}(4m_t^2,M_W^2,M_W^2)\Bigg],\end{aligned} \tag{A.1}$$

where $Q_b = -1/3$ is bottom quark electric charge normalized to the one of positron. The corresponding contribution to the wave function renormalization constant reads

$$Z_2^{(1,0)} = \frac{\alpha}{4\pi s_w^2}\left[\left(1+2\,(1-\epsilon)\,z\right)\frac{A_0^{(\epsilon)}\left(M_W^2\right)}{8M_W^2} - \frac{(1+z)\left(1+2\,(1-\epsilon)\,z\right)}{8z}B_0^{(\epsilon)}(m_t^2,M_W^2,0)\right.$$
$$\left. -\frac{(1-z)\left(1+2\,(1-\epsilon)\,z\right)}{4z}\left\{m_t^2\frac{\partial}{\partial m_t^2}B_0^{(\epsilon)}(m_t^2,M_W^2,0)\right\}\right]. \tag{A.2}$$

The loop-functions $A_0^{(\epsilon)}$ and $B_0^{(\epsilon)}$ are given by

$$A_0^{(\epsilon)}(M_W^2)/M_W^2 = -\left(\frac{e^{\gamma_E}\mu^2}{M_W^2}\right)^{\epsilon}\Gamma(-1+\epsilon)\,, \tag{A.3}$$

$$B_0^{(\epsilon)}(4m_t^2,0,0) = \left(-\frac{e^{\gamma_E}\mu^2}{m_t^2}\right)^{\epsilon}\frac{\sqrt{\pi}\,\Gamma(\epsilon)\,\Gamma(1-\epsilon)}{2\,\Gamma(\frac{3}{2}-\epsilon)}\,, \tag{A.4}$$

$$B_0^{(\epsilon)}(m_t^2,M_W^2,0) = \left(\frac{e^{\gamma_E}\mu^2}{m_t^2}\right)^{\epsilon}\left(-1+\frac{M_W^2}{m_t^2}\right)^{-\epsilon}\frac{\Gamma(\epsilon)}{1-\epsilon}$$
$$\times\,{}_2F_1\left(\epsilon,1-\epsilon,2-\epsilon;\,1/(1-M_W^2/m_t^2)\right), \tag{A.5}$$

$$B_0^{(\epsilon)}(4m_t^2,M_W^2,M_W^2) = \frac{1}{2(1-\epsilon)}\left(\frac{e^{\gamma_E}\mu^2}{2M_W^2}\right)^{\epsilon}\Gamma(\epsilon)\times\left[\left(1-\frac{1}{\sqrt{1-\frac{M_W^2}{m_t^2}}}\right)^{\epsilon}\left(1+\sqrt{1-\frac{M_W^2}{m_t^2}}\right)\right.$$
$$\times\,{}_2F_1\left(1-\epsilon,\epsilon,2-\epsilon;\frac{1}{2}\left(1+\frac{1}{\sqrt{1-\frac{M_W^2}{m_t^2}}}\right)\right)$$
$$+\left(1+\frac{1}{\sqrt{1-\frac{M_W^2}{m_t^2}}}\right)^{\epsilon}\left(1-\sqrt{1-\frac{M_W^2}{m_t^2}}\right)$$
$$\left.\times\,{}_2F_1\left(1-\epsilon,\epsilon,2-\epsilon;\frac{1}{2}\left(1-\frac{1}{\sqrt{1-\frac{M_W^2}{m_t^2}}}\right)\right)\right], \tag{A.6}$$

where an analytic continuation by (m_t^2+i0) is understood. Expansions with respect to ϵ of the Gauss-hypergeometric functions ${}_2F_1$ around integer values is well known in the literature (see, e.g., ref. [39] or the package HypExp [52]).

B. Unstable top quarks

In this appendix we briefly review our treatment of unstable particle effects for the hard vertex corrections to the top quark production near threshold. For a more general framework we refer to refs. [53, 54].

The threshold cross section is sensitive to scales of order Γ_t. Thus it is mandatory to incorporate the unstable particle effects to obtain physically meaningful results. However, there are several conceptual questions, e.g., the treatment of the imaginary part of the wave

JHEP01(2009)038

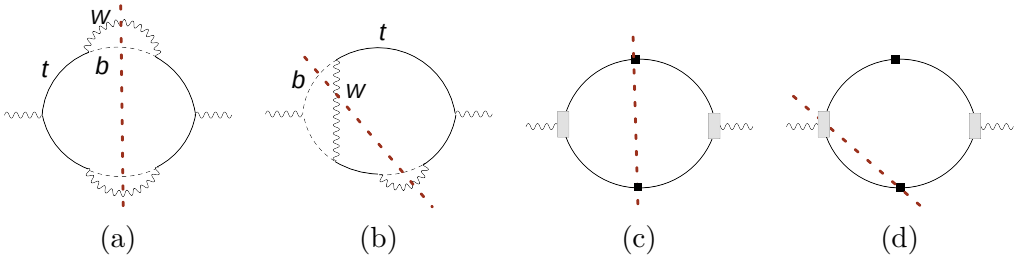

Figure 8: Electroweak corrections involving top quarks to the photon vacuum polarization ((a) and (b)). The corresponding NRQCD Feynman diagrams are shown in (c) and (d). The solid lines represent the top quark, dashed and wavy lines denote bottom quarks and W bosons, respectively. The dotted lines represent the cuts corresponding to top quark decay, $t \to bW$. In (c) and (d) the square vertex and black dot on the top quark line represent the $\gamma t\bar{t}$ vertex and top quark propagators in NRQCD, respectively.

function renormalization for the unstable top quarks. This occurs when unstable particles appear in the external lines of the S-matrix element. An obvious solution to the problems is to discuss the unstable particle production together with its subsequent decay, so that no unstable particles appear as external lines of the Feynman diagrams. This is consistent with the experimental situation where we measure the decay products of the top quarks in the detectors. For our purpose it is sufficient to consider W bosons and bottom quarks as stable.

In the following we will show how top quark production near threshold is formulated from the point of view of the optical theorem.[11] To this end we consider resonant top quark correction to the photon vacuum polarization which reads

$$\Pi(q) \sim \int \frac{d^dp}{(2\pi)^d i}\, \Gamma_1\, \frac{Z_2^{\rm ew}}{(p+q/2)^2 - m_t^2 + im_t\Gamma_t}\, \Gamma_2\, \frac{Z_2^{\rm ew}}{(p-q/2)^2 - m_t^2 + im_t\Gamma_t}\,, \quad \text{(B.1)}$$

where $q = (\sqrt{s},\ \vec{0})$, m_t and Γ_t is a pole mass and decay width of top quark, and $\Gamma_{1,2}$ represent the $\gamma t\bar{t}$ vertex including radiative corrections. In the above expression the full propagators for the top and anti-top quarks are employed (i.e. Dyson resummation of electroweak self energy diagrams has been performed), and an expansion around $(p \pm q/2)^2 \simeq m_t^2$ is performed. This expansion picks up the leading behaviour of the threshold cross section near $\sqrt{s} \sim 2m_t$. Two sample Feyman diagrams contributing to $\Pi(q)$ are shown in figure 8 (a) and (b).

We are interested in specific cuts of the $\Pi(q)$ which correspond to the process

$$\gamma^* \to t\bar{t} \to (b\,W^+)\ (\bar{b}\,W^-)\,. \quad \text{(B.2)}$$

The first diagram in figure 8 with the cut indicated by the dotted line is an example for a contribution to eq. (B.2) where the invariant mass of the top and anti-top quarks are slightly off shell due to their finite width, i.e. $p_t^2 - m_t^2 \sim m_t\,\Gamma_t$. By the same reason the cut

[11] Since for our argument the spinor structure is irrelevant we discuss only the scalar part of the Feynman diagrams in what follows.

of the diagram in figure 8(b) should also be regarded as a contribution to the top quark production due to the interference of the processes

$$\gamma^* \to t\bar{t} \to (b\,W^+)\;(\bar{b}\,W^-) \qquad \text{and} \qquad \gamma^* \to (b\,W^+)\bar{t} \to (b\,W^+)\;(\bar{b}\,W^-)\,, \tag{B.3}$$

as long as the invariant mass of the bottom quark and W boson mass satisfies $(p_b + p_W)^2 - m_t^2 \sim m_t\Gamma_t$. Once the finite width effects are included into the theory calculation this is an automatic consequence. Furthermore gauge invariance requires to also take into account such interference terms [13].

In a next step the vacuum polarization in the SM has to be matched to the one in NRQCD. At zeroth order in QCD the two diagrams (a) and (b) in figure 8 are matched to the NRQCD Feynman diagrams (c) and (d). NRQCD reproduces the on-shell behaviour of the renormalized top quark propagator including the width Γ_t, while the effect of the wave function Z_2 due to W boson exchange is not present in the NRQCD Lagrangian. Thus we absorb both the real and imaginary part of Z_2 into the vertex correction, which is treated as an external current in NRQCD. In this manner the vacuum polarization is written as

$$\begin{aligned}\Pi_{\text{NRQCD}}(q) \sim \int \frac{d^dp}{(2\pi)^d i}\;\Big[\hat{\Gamma}_1\Big]_{\vec{p}=0}\;\frac{1}{2m_t}\;\frac{1}{p^0+\frac{q^0}{2}-m_t-\frac{\vec{p}^{\,2}}{2m_t}+i\frac{\Gamma_t}{2}}\;\Big[\hat{\Gamma}_2\Big]_{\vec{p}=0}\\ \times\frac{1}{2m_t}\;\frac{1}{-p^0+\frac{q^0}{2}-m_t-\frac{\vec{p}^{\,2}}{2m_t}+i\frac{\Gamma_t}{2}}\;+\ldots\,,\end{aligned} \tag{B.4}$$

where $[\hat{\Gamma}_i]_{\vec{p}=0} \equiv Z_2\Gamma_{1,2}|_{\vec{p}=0}$ is the renormalized vertex corrections at $\vec{p}=0$. For the vacuum polarization in NRQCD the hard vertex corrections are expanded in the small momentum $\vec{p}$, and the higher order terms from $\hat{\Gamma}_{1,2}$ and the full propagators should be systematically incorporated order by order in the NRQCD framework to maintain renormalizability.

Hence, we arrived at hard vertex corrections $[\hat{\Gamma}_{1,2}]_{\vec{p}=0}$ which are renormalized using on-shell wave function factors represented by square vertices in figure 8. In figure 8 the black dots on the top quark line contain the $i\Gamma_t$ term, which is responsible for the imaginary part of the NRQCD propagators. Note that the W boson correction to the top quark propagator generates both the imaginary part of Z_2 and $i\Gamma_t$ in the diagrams (a) and (b) while in the NRQCD Feyman diagrams (c) and (d), only the term of $i\Gamma_t$ is reproduced. Thus Z_2, including its imaginary part, should be taken into account in the computation of the vertices.

References

[1] M. Martinez and R. Miquel, *Multi-parameter fits to the t anti-t threshold observables at a future e^+e^- linear collider*, *Eur. Phys. J.* **C 27** (2003) 49 [hep-ph/0207315].

[2] G.T. Bodwin, E. Braaten and G.P. Lepage, *Rigorous QCD analysis of inclusive annihilation and production of heavy quarkonium*, *Phys. Rev.* **D 51** (1995) 1125 [*Erratum ibid.* **D 55** (1997) 5853] [hep-ph/9407339].

[3] A.H. Hoang et al., *Top-antitop pair production close to threshold: synopsis of recent NNLO results*, *Eur. Phys. J. Direct.* **C 2** (2000) 1 [hep-ph/0001286].

[4] M. Beneke, Y. Kiyo and K. Schuller, *NNNLO results on top-quark pair production near threshold*, PoS(RAD COR 2007)051 [arXiv:0801.3464].

[5] M. Beneke, Y. Kiyo and A.A. Penin, *Ultrasoft contribution to quarkonium production and annihilation*, *Phys. Lett.* **B 653** (2007) 53 [arXiv:0706.2733];
M. Beneke and Y. Kiyo, *Ultrasoft contribution to heavy-quark pair production near threshold*, *Phys. Lett.* **B 668** (2008) 143 [arXiv:0804.4004].

[6] A.H. Hoang, *Top Pair Production at Threshold and Effective Theories*, *Acta Phys. Polon.* **B34** (2003) 4491 [hep-ph/0310301].

[7] A. Pineda and A. Signer, *Heavy quark pair production near threshold with potential non-relativistic QCD*, *Nucl. Phys.* **B 762** (2007) 67 [hep-ph/0607239].

[8] R.J. Guth and J.H. Kuhn, *Top quark threshold and radiative corrections*, *Nucl. Phys.* **B 368** (1992) 38.

[9] A.H. Hoang and C.J. Reisser, *On electroweak matching conditions for top pair production at threshold*, *Phys. Rev.* **D 74** (2006) 034002 [hep-ph/0604104].

[10] D. Eiras and M. Steinhauser, *Complete Higgs mass dependence of top quark pair threshold production to order $\alpha\alpha_s$*, *Nucl. Phys.* **B 757** (2006) 197 [hep-ph/0605227].

[11] B.A. Kniehl, *Two Loop Corrections to the Vacuum Polarizations in Perturbative QCD*, *Nucl. Phys.* **B 347** (1990) 86.

[12] A. Djouadi and P. Gambino, *Electroweak gauge bosons selfenergies: complete QCD corrections*, *Phys. Rev.* **D 49** (1994) 3499 [*Erratum ibid.* **D 53** (1996) 4111] [hep-ph/9309298].

[13] A.H. Hoang and C.J. Reisser, *Electroweak absorptive parts in NRQCD matching conditions*, *Phys. Rev.* **D 71** (2005) 074022 [hep-ph/0412258].

[14] M.E. Luke and M.J. Savage, *Power counting in dimensionally regularized NRQCD*, *Phys. Rev.* **D 57** (1998) 413 [hep-ph/9707313].

[15] M. Beneke and V.A. Smirnov, *Asymptotic expansion of Feynman integrals near threshold*, *Nucl. Phys.* **B 522** (1998) 321 [hep-ph/9711391].

[16] A. Pineda and J. Soto, *Effective field theory for ultrasoft momenta in NRQCD and NRQED*, *Nucl. Phys.* **64** *(Proc. Suppl.)* (1998) 428 [hep-ph/9707481].

[17] N. Brambilla, A. Pineda, J. Soto and A. Vairo, *Potential NRQCD: an effective theory for heavy quarkonium*, *Nucl. Phys.* **B 566** (2000) 275 [hep-ph/9907240].

[18] B.A. Kniehl, A.A. Penin, V.A. Smirnov and M. Steinhauser, *Potential NRQCD and heavy-quarkonium spectrum at next-to- next-to-next-to-leading order*, *Nucl. Phys.* **B 635** (2002) 357 [hep-ph/0203166].

[19] A.V. Smirnov, V.A. Smirnov and M. Steinhauser, *Fermionic contributions to the three-loop static potential*, *Phys. Lett.* **B 668** (2008) 293 [arXiv:0809.1927].

[20] V.S. Fadin and V.A. Khoze, *Threshold Behavior of Heavy Top Production in e^+e^- Collisions*, *JETP Lett.* **46** (1987) 525 [*Pisma Zh. Eksp. Teor. Fiz.* **46** (1987) 417].

[21] A.A. Penin and A.A. Pivovarov, *Analytical results for $e^+e^- \to$ t anti-t and gamma gamma $\to$ t anti-t observables near the threshold up to the next-to-next-to-leading order of NRQCD*, *Phys. Atom. Nucl.* **64** (2001) 275 [*Yad. Fiz.* **64** (2001) 323] [hep-ph/9904278].

JHEP01(2009)038

[22] B.A. Kniehl and A.A. Penin, *Ultrasoft effects in heavy quarkonium physics*, *Nucl. Phys.* **B 563** (1999) 200 [hep-ph/9907489].

[23] A.V. Manohar and I.W. Stewart, *Running of the heavy quark production current and 1/k potential in QCD*, *Phys. Rev.* **D 63** (2001) 054004 [hep-ph/0003107].

[24] B.A. Kniehl, A.A. Penin, M. Steinhauser and V.A. Smirnov, *Heavy-quarkonium creation and annihilation with $O(\alpha_s^3 \ln(\alpha_s))$ accuracy*, *Phys. Rev. Lett.* **90** (2003) 212001 [*Erratum ibid.* **91** (2003) 139903] [hep-ph/0210161].

[25] A.H. Hoang, *Three-loop anomalous dimension of the heavy quark pair production current in non-relativistic QCD*, *Phys. Rev.* **D 69** (2004) 034009 [hep-ph/0307376].

[26] A.A. Penin, V.A. Smirnov and M. Steinhauser, *Heavy quarkonium spectrum and production/annihilation rates to order $\beta_0^3\alpha_s^3$*, *Nucl. Phys.* **B 716** (2005) 303 [hep-ph/0501042].

[27] A. Czarnecki and K. Melnikov, *Two-loop QCD corrections to the heavy quark pair production cross section in e^+e^- annihilation near the threshold*, *Phys. Rev. Lett.* **80** (1998) 2531 [hep-ph/9712222].

[28] M. Beneke, A. Signer and V.A. Smirnov, *Two-loop Correction to the Leptonic Decay of Quarkonium*, *Phys. Rev. Lett.* **80** (1998) 2535 [hep-ph/9712302].

[29] P. Marquard, J.H. Piclum, D. Seidel and M. Steinhauser, *Fermionic corrections to the three-loop matching coefficient of the vector current*, *Nucl. Phys.* **B 758** (2006) 144 [hep-ph/0607168].

[30] P. Nogueira, *Automatic Feynman Graph Generation*, *J. Comput. Phys.* **105** (1993) 279.

[31] R. Harlander, T. Seidensticker and M. Steinhauser, *Complete corrections of $O(\alpha\alpha_s)$ to the decay of the Z boson into bottom quarks*, *Phys. Lett.* **B 426** (1998) 125 [hep-ph/9712228].

[32] T. Seidensticker, *Automatic application of successive asymptotic expansions of Feynman diagrams*, hep-ph/9905298.

[33] P. Marquard and D. Seidel, *Crusher: a C++ implementation of the Laprota algorithm*, unpublished.

[34] S. Laporta and E. Remiddi, *The analytical value of the electron (g-2) at order α^3 in QED*, *Phys. Lett.* **B 379** (1996) 283 [hep-ph/9602417].

[35] S. Laporta, *High-precision calculation of multi-loop Feynman integrals by difference equations*, *Int. J. Mod. Phys.* **A 15** (2000) 5087 [hep-ph/0102033].

[36] R. Scharf and J.B. Tausk, *Scalar two loop integrals for gauge boson selfenergy diagrams with a massless fermion loop*, *Nucl. Phys.* **B 412** (1994) 523.

[37] J. Fleischer, F. Jegerlehner, O.V. Tarasov and O.L. Veretin, *Two-loop QCD corrections of the massive fermion propagator*, *Nucl. Phys.* **B 539** (1999) 671 [*Erratum ibid.* **B 571** (2000) 511] [hep-ph/9803493].

[38] D. Seidel, *Analytic two-loop virtual corrections to $b \to d\,\ell^+\ell^-$*, *Phys. Rev.* **D 70** (2004) 094038 [hep-ph/0403185].

[39] M.Y. Kalmykov, *Gauss hypergeometric function: reduction, ϵ-expansion for integer/half-integer parameters and Feynman diagrams*, *JHEP* **04** (2006) 056 [hep-th/0602028].

JHEP01(2009)038

[40] J.H. Piclum, *Heavy quark threshold dynamics in higher order*, Ph.D. Thesis, Hamburg University (2007).

[41] M. Argeri and P. Mastrolia, *Feynman Diagrams and Differential Equations*, *Int. J. Mod. Phys.* **A 22** (2007) 4375 [arXiv:0707.4037].

[42] E. Remiddi and J.A.M. Vermaseren, *Harmonic polylogarithms*, *Int. J. Mod. Phys.* **A 15** (2000) 725 [hep-ph/9905237].

[43] V.A. Smirnov, *Evaluating Feynman Integrals*, *Springer Tracts Mod. Phys.* **211** (2004) 1.

[44] J. Gluza, K. Kajda and T. Riemann, *AMBRE: a Mathematica package for the construction of Mellin-Barnes representations for Feynman integrals*, *Comput. Phys. Commun.* **177** (2007) 879 [arXiv:0704.2423].

[45] M. Czakon, *Automatized analytic continuation of Mellin-Barnes integrals*, *Comput. Phys. Commun.* **175** (2006) 559 [hep-ph/0511200].

[46] T. Hahn, *CUBA: a library for multidimensional numerical integration*, *Comput. Phys. Commun.* **168** (2005) 78 [hep-ph/0404043].

[47] A.V. Smirnov and M.N. Tentyukov, *Feynman Integral Evaluation by a Sector decomposiTion Approach (FIESTA)*, arXiv:0807.4129.

[48] A. Denner, *Techniques for calculation of electroweak radiative corrections at the one loop level and results for W physics at LEP-200*, *Fortschr. Phys.* **41** (1993) 307 [arXiv:0709.1075].

[49] LEP Electroweak Working Group (LEP EWWG), see http://lepewwg.web.cern.ch/LEPEWWG.

[50] Tevatron Electroweak Working Group collaboration and others, *Combination of CDF and D0 Results on the Mass of the Top Quark*, arXiv:0808.1089.

[51] D. Eiras and M. Steinhauser, *Two-loop $O(\alpha\alpha_s)$ corrections to the on-shell fermion propagator in the standard model*, *JHEP* **02** (2006) 010 [hep-ph/0512099].

[52] T. Huber and D. Maître, *HypExp 2, Expanding Hypergeometric Functions about Half- Integer Parameters*, *Comput. Phys. Commun.* **178** (2008) 755 [arXiv:0708.2443].

[53] M. Beneke, A.P. Chapovsky, A. Signer and G. Zanderighi, *Effective theory approach to unstable particle production*, *Phys. Rev. Lett.* **93** (2004) 011602 [hep-ph/0312331].

[54] M. Beneke, P. Falgari, C. Schwinn, A. Signer and G. Zanderighi, *Four-fermion production near the W pair production threshold*, *Nucl. Phys.* **B 792** (2008) 89 [arXiv:0707.0773].

JHEP01(2009)038